



www.DeepakPublishing.com

Patmont, C. et al. (2016): JoSS, Vol. 5, No. 1, pp. 407–418
(Peer-reviewed article available at www.jossonline.com)



www.JoSSonline.com

Design and Characterization of a Spring Steel Hinge for Deployable CubeSat Structures

Elbara Ziade, Calvin S. Patmont, and Theodore A. Fritz

*Department of Mechanical Engineering and Center for Space Physics, Boston University
Boston, MA, USA*

Abstract

A novel implementation of a spring steel was used to design an economical, self-locking, self-guiding, and self-actuating single-component hinge. The concept behind the hinge is an off-planar arrangement of commercial off-the-shelf (COTS) spring steel strips. The off-plane arrangement of the spring steel strips creates asymmetric folding and buckling to provide the necessary stiffness and dampening for solar panel deployment. This paper presents four spring steel hinge configurations and the analytic equations used to characterize them from three solar panel mass deployments in microgravity. It also discusses the forces generated by the hinge and energy dissipation rate for representative model systems.

1. Introduction

University-developed CubeSat specifications have already demonstrated the broad impact that a simple, robust and modular satellite bus has on institutional and private industry spaceflight endeavors (Straub, 2012). In addition, the economic benefits of configuring and qualifying commercial off-the-shelf (COTS) technology for space applications continues to increase the popularity of CubeSat missions and satellite groups' accessibility to space (Skrobot, 2011; Skrobot and Coelho, 2012).

As CubeSats evolve, their electronic and instrument complexity increases, demanding more power to achieve more sophisticated endeavors. The con-

strained power budget must be met by using either more efficient solar cells, or by incorporating deployable solar panels to increase the sun-facing surface area. Resource-constrained small satellite teams design in-house solar panel deployment systems because available space-rated COTS deployment systems are too expensive, and are also sold as complete packages, which restricts CubeSat design configurations.

The current study's response to this barrier of entry for deployment systems is the design and characterization of a scalable and configurable hinge for the CubeSat bus. The simple-continuous or "solid-state" nature of this mechanical design needs fewer qualifications than pinned joint hinge alternatives, which are affected by thermal expansion, galling, cold

Corresponding Author: Calvin S. Patmont, cpatmont@bu.edu

welding, and lubrication in a vacuum environment. Through a novel off-planar arrangement of COTS spring steel strips, the authors have designed a self-actuating, self-guiding, and self-locking hinge, while simultaneously circumventing the risks associated with the pinned-joint scheme.

This paper investigates the dynamic response of the solid-state spring steel hinge to find the maximum forces placed on the spacecraft from deployment, characterizing stiffness and dampening properties. These goals are obtained through dynamic tests on a NASA reduced gravity flight, and inverse-problem analysis on typical 1U, 3U, and 6U CubeSat solar panel form-factors. In addition, this study demonstrates the implementation of the hinge design on a 6U CubeSat, called ANDESITE, under development at Boston University.

2. Design and Manufacture of a Spring Steel Hinge

2.1. Legacy Hinge Designs

Satellites have demonstrated the ability to reliably deploy solar panels to meet their power budgets. From deployment successes, hinge designs matured into two categories: the “rigid” hinge and the “flexible” hinge.

The rigid hinge is similar to a door hinge modified for space applications, and contains three distinct components: 1) a pin and housing for the solar panel to pivot around; 2) a torsional spring to provide the force for deployment; and 3) a latching mechanism to lock the panel in place (Honeybee Robotics, 2006).

The flexible hinge uses the steel tape from a carpenter tape measure, and incorporates two housings separated by one or more carpenter tape shells. The curved nature of the tape shells provides the restoring force to deploy and lock the solar panel into position (the least energy state of the tape spring). The carpenter tape is in its buckled state when the solar panel is stowed for the launch vehicle. Seffen and Pellegrino have characterized carpenter tape for solar panel and antenna deployments (Seffen and Pellegrino, 1997, 1999; S. Pellegrino and Watt, 2002). In addition, Sicre et al. (J. Sicre et al., 2005) and Lathuiliere et al. (M.

Lathuiliere, 2009) designed and characterized a carpenter tape configuration, named Maeva, for a solar array and boom deployment on their satellite DEMETER. The economical and configurable CubeSat hinge designed in this study was inspired by the work from these groups.

2.2. Design Basis

An important aspect of the hinge characterized in this paper is the student-run CubeSat program’s ability to design, manufacture, and assemble all hinge components in-house. The material cost of the hinge was less than \$30 USD, and students performed all machining in a university machine shop using a 2.5 axis CNC and a 1/8-inch ball endmill.

The purpose of the novel design is to overcome the drawbacks found in the fixed and flexible configurations:

- The rigid hinge runs the risk of cold welding and galling between joint contacts during launch. Therefore, deployment tests of the rigid hinge in a thermal-vacuum environment are required and often not available to student CubeSat groups. The time-costs of environmental testing are not in line with the quick development time and student turnover rates inherent to university CubeSat programs.
- The spring steel used in the flexible hinge design is stripped from hardware store carpenter tape measures and lack material specifications. Moreover, the flexible hinges that have been previously characterized are too large for CubeSat applications.

This design, referred to as the solid-state hinge, uses two AISI 1095 spring steel strips oriented in an off-planar arrangement. The coincident ends of each strip mount with mechanical fasteners and space-rated epoxy into aluminum housings. The off-planar angle generates buckling and bending modes, resulting in a self-guiding, self-actuating, and self-locking hinge due to the asymmetric deformation of the strips during deployment. Unlike the fixed hinge, which moves to the deployed 0° position in a single movement and abruptly locks in that position, the solid-state hinge

dissipates stored potential energy by oscillating through the deployed position until dampening completes. Desired deployment characteristics for a range of solar panel masses are tuned by adjusting three configuration parameters: thickness, off-planar angle, and length (see Figure 1). The primary focus of this

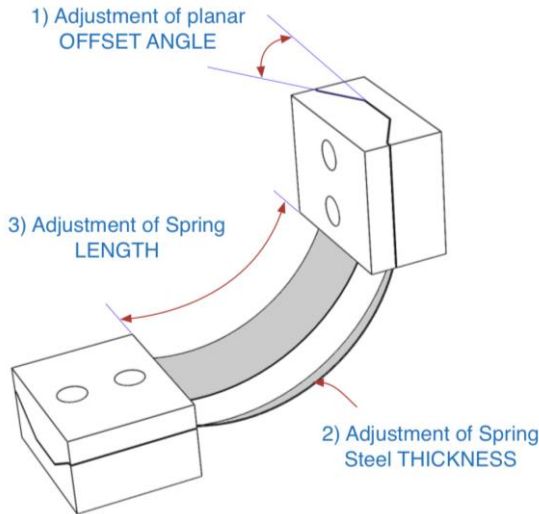


Figure 1. Sketch of hinge design with the three tuneable aspects.

paper covers off-angle adjustments and a thickness adjustment. Table 1 lists the tested hinge configurations.

Table 1. Solid-State Hinge Test Parameters

Spring Steel Offset Angles	0°, 15°, 30°, 45°
Spring Steel Thicknesses	.005 in. and .007 in.

Due to the CubeSat’s small envelope requirements for launch, spring steel strips were selected, to reduce the profile of the hinge design. The narrowest COTS spring steel were found to be .25 inches wide, and the thinnest spring steel at this width was .005 inches thick. Preliminary lab tests objectively determined the most interesting offset angles to be between 0 and 45 degrees.

3. Dynamic Testing

3.1. Experimental Overview

The current research studied the dynamic effects of four solid-state hinge prototypes in a microgravity

environment. A test rig was prepared to record deployment angle versus time of the hinge configurations on three solar panel masses. From this data, three characteristics can be derived from each simulation: spring stiffness, settling time, and general dynamic trends.

The dynamic test rig used is a 75 in. x 27 in. x 40 in. structure constructed primarily of 80/20 extruded aluminum for ease of transportation, quick assembly, and strength—all of which are necessary for testing on the NASA C-9 parabolic aircraft (see Figure 2 for a CAD model of the rig and Figure 3 for a photo of the

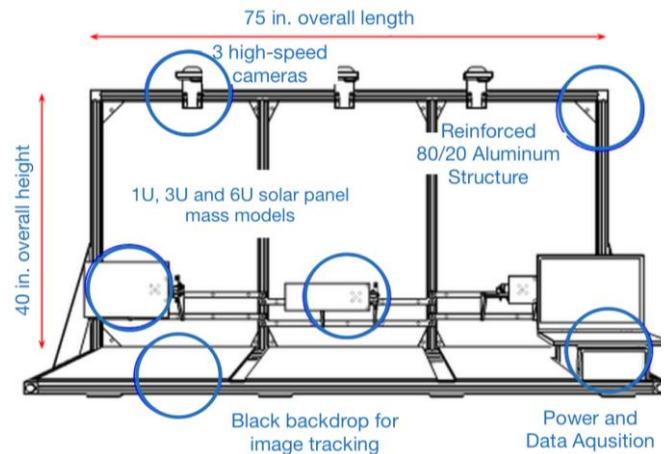


Figure 2. Sketch of the dynamic test rig.

assembled rig on the NASA aircraft). Three solar panel masses can be deployed simultaneously during the 0G portion of each parabola. The 1U, 3U, and 6U representative models match mass and geometry of functional CubeSat solar panels (ClydeSpace, 2014; GOMSpace, 2014) and minimize drag due to air resistance found in the testing environment. High-speed cameras mounted to the structure captured the motion of the three deployments.

Prior to flight, the apparatus was verified on the ground. To counteract the forces due to gravity, lightweight mono-filament line was attached to each solar panel near the pivot point and secured to the ceiling approximately ten feet above. The long mono-filament line displaced the solar panels less than 0.04 inches out of the deployment plane—an amount that had no noticeable impact on deployment characteristics.

To characterize a range of solid-state hinge angle and thickness configurations in the allotted time-frame

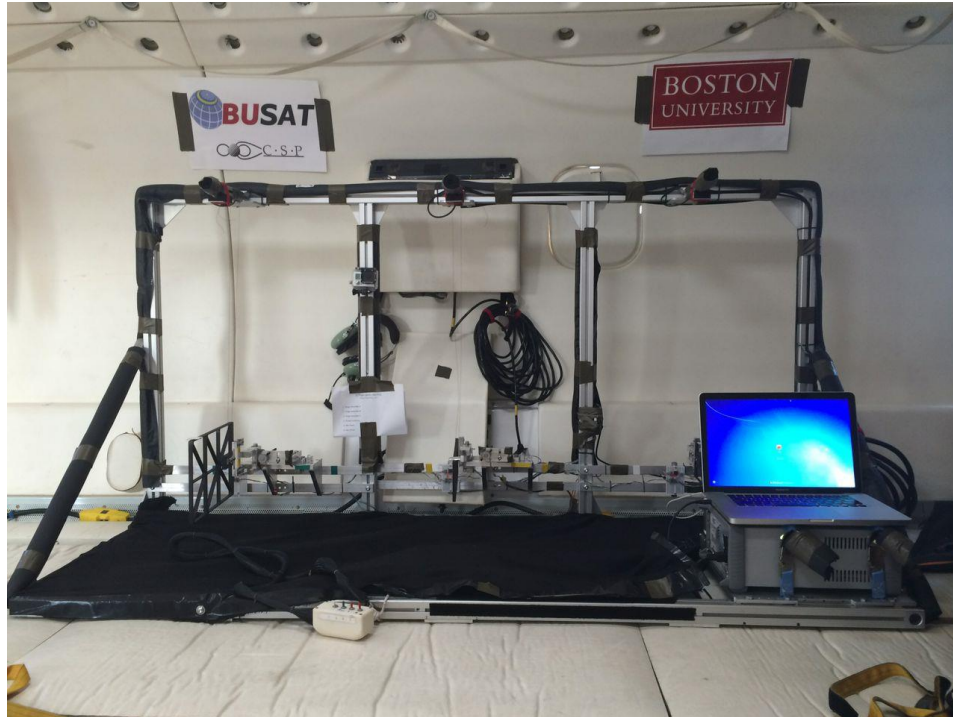


Figure 3. The dynamic test rig on board the NASA C-9 microgravity aircraft.

provided by the microgravity flights, hinge parameters were selected that will provide the maximum insight into the solid-state hinge variables. Four hinge angles, three solar panel masses, and two spring-steel thicknesses were selected, allowing for testing of the full range of possible hinge angles, the three common CubeSat solar panel masses, and two thicknesses to study the effect of increases spring rigidity on the dynamic response of the system.

Table 2 presents the microgravity test schedule, which outlines the specific hinge setups used. This paper refers to the configurations by their solar panel size and degree angle in the format of 3U15D, where 3U is a 3U solar panel mass and 15D is a 15° angled hinge.

3.2. Data Acquisition and Image Processing

Three Go-Pro cameras captured the deployment at 240 frames-per-second with 848x480 pixel resolution. The Nyquist sampling theorem suggests that the high-speed cameras can record a maximum oscillation frequency of 120Hz and still provide meaningful results—an order of magnitude higher than any deployment encountered in this study.

The software program Adobe After Effects was used to crop and convert the images to grayscale for MATLAB object-tracking algorithms. Tracking errors were minimized by placing a highly reflective tracker on the solar panels. Figure 4 illustrates the image

Table 2. Microgravity Solid-State Hinge Test Schedule

Flight No.	Number of Parabolas	6U Panel	3U Panel	1U Panel
Flight 1	20	30°, 0.005 in.	15°, 0.005 in.	0°, 0.005 in.
Flight 2	20	45°, 0.005 in.	30°, 0.005 in.	15°, 0.005 in.
Flight 3	20	30°, 0.007 in.	45°, 0.005 in.	30°, 0.005 in.
Flight 4	20	15°, 0.005 in.	30°, 0.007 in.	45°, 0.005 in.

tracking operations and plots for angular position, velocity, and acceleration for a single deployment.

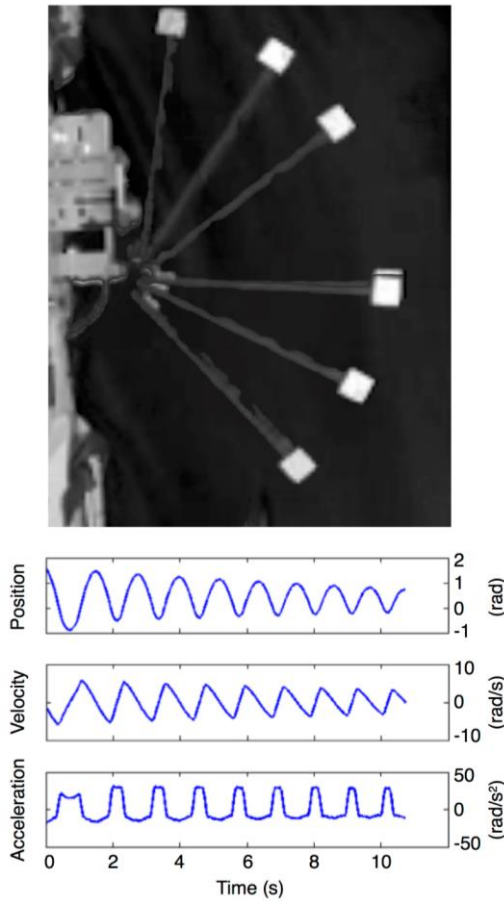


Figure 4. Top: Seven discrete images taken from video to visualize the MATLAB image tracking algorithm; Bottom, from top to bottom: Position, velocity, and acceleration plots for 3U15D configuration.

4. Results and Analysis

4.1. Spring Stiffness Methods

The force imparted on the spacecraft by the solid-state hinge during deployment is proportional to the spring stiffness as stated by a nonlinear version of Hooke's Law:

$$F_{max} = -K_{spring}(x) \times x_{stowed}$$

where x is the displacement of the solar panel mass with respect to the fully deployed position. Appropri-

ate sizing of this force F_{max} , and therefore overall stiffness K_{spring} , impacts spacecraft attitude in two ways. A large stiffness may exceed the spacecraft's Attitude Determination and Control System's (ADCS) ability to recover from the deployment shock in an adequate time-frame. A small stiffness coincides with a low dampening coefficient, which may experience a long settling time and reduce mission lifetime. Because ADCS simulations use maximum forces imparted on the satellite, this analysis focused on early deployment forces in the first oscillation.

Two methods were used to calculate the spring stiffness, and the two results were compared for consistency. The goal of this analysis was to gain insight about the effects of varying offset angle, thickness, and solar panel mass. For simplicity, a linear spring model was used and the data were analyzed in discrete time intervals, thus minimizing the deviation of the linear model to the non-linear behavior of the hinge system. The non-linear behaviors are addressed in Section 5.2 of this paper.

4.2. Empirical Stiffness Calculation

The average stiffness of the hinge from stowed to halfway through the first oscillation was estimated using the law of Conservation Of Energy (COE). This analysis assumed that no energy is lost when the solar panel moves from the stowed position, 90° , through the first pass of the deployed position, 0° . This assumption provided a lower bound, because it neglects energy lost due to dampening, which reduces the angular velocity of the solar panel mass. For simplicity, the energy stored in the hinge was defined with the equation for potential energy of a linear spring: $\frac{1}{2}kx_{stowed}^2$. The maximum potential energy of the system was defined as the moment the angular velocity of the solar panel mass is maximum, or when the solar panel mass passes through the first deployed position: $\frac{1}{2}I\dot{x}_{origin}^2$, where I is the mass-moment of inertia for each solar panel mass and \dot{x} is the angular velocity. Because it was assumed that no energy is lost from the stowed position through the first deployment, kinetic energy is set equal to the potential energy and an

estimated lower bound of stiffness for the hinge system was calculated from Equation 1. This analysis found that the energy stored increased with off-set angle and thickness of the spring steel hinge. Additionally, the stiffness was found to be constant among mass models within 20% as shown in Figure 5.

$$\frac{1}{2}I\dot{x}_{origin}^2 = \frac{1}{2}kx_{stowed}^2 \quad (1)$$

The stiffness coefficient in Equation 1 is compared with the stiffness of the first oscillation from the linear mass-spring-dashpot ordinary differential equation (ODE). Dampening is considered this time to provide an upper bound to the stiffness values.

$$m\ddot{x} + c\dot{x} + kx = 0 \quad (2)$$

The over-defined system was conditioned to find stiffness and dampening coefficients using matrix algebra. First, the position data x for an oscillation was

differentiated numerically to find velocity \dot{x} and acceleration \ddot{x} . These were compiled into a linear system in the form of Equation 2, then the stiffness and dampening coefficients were normalized, and \ddot{x} was subtracted from both sides to get to the system of equations shown below as Equation 3.

$$\begin{bmatrix} \dot{x}_1 & x_1 \\ \dot{x}_2 & x_2 \\ \dot{x}_3 & x_3 \\ \vdots & \vdots \\ \dot{x}_n & x_n \end{bmatrix} \begin{Bmatrix} \frac{c}{m} \\ \frac{k}{m} \end{Bmatrix} = \begin{bmatrix} \ddot{x}_1 \\ \ddot{x}_2 \\ \ddot{x}_3 \\ \vdots \\ \ddot{x}_n \end{bmatrix} \quad (3)$$

$$\begin{bmatrix} X \end{bmatrix} \begin{Bmatrix} K \end{Bmatrix} = \begin{bmatrix} A \end{bmatrix} \quad (4)$$

$$K = X^+A$$

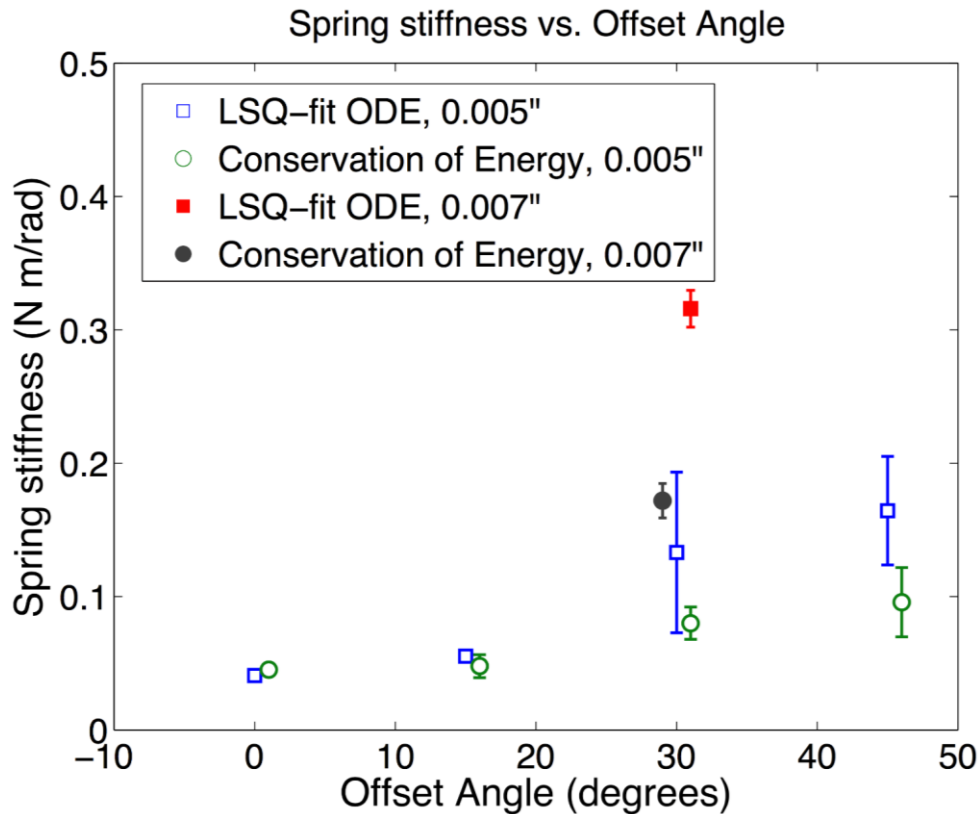


Figure 5. Stiffness vs. offset angle of the spring steel strips. The open markers are for the thin spring steel sheet, and the filled markers represent the thicker spring strips sheet. Error bars represent one standard deviation of fitted data.

Equation 3 is solved for $[K]$ using the Moore-Penrose pseudoinverse method (shown in Equation 4), resulting in the least-squared values of the normalized stiffness $\frac{k}{m}$ and damping coefficients $\frac{c}{m}$.

Figure 5 is a plot of the derived stiffness k from the two methods, versus hinge offset angle. The k values for each offset angle are averaged across the three solar masses, because spring stiffness is independent of mass for a linear oscillator.

Two trends are observed: First, stiffness increases with spring steel thickness; and second, the stiffness of the solid-state hinge increases with offset angle. These phenomena occur from *simple beam* bending mechanics (R. Juvinall, 2012):

$$K = \frac{EI}{L} \tag{5}$$

where I is the moment of inertia for the beam, E is the Young’s modulus of spring steel (200GPa), and L is the strip length. I is defined in Figure 6 as a rectangular bar rotated by an angle θ . An increase in the spring

$$I = \frac{wt}{12} (t^2 \cos^2 \theta + w^2 \sin^2 \theta)$$

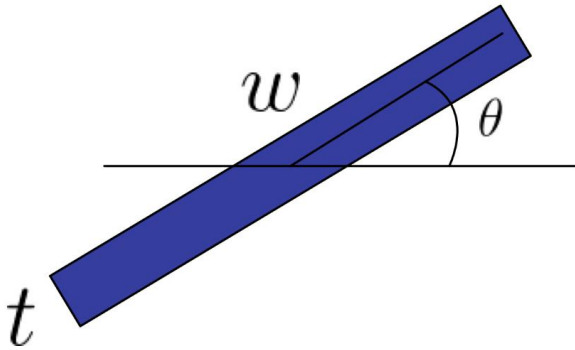


Figure 6. Mass Moment of Area formula for a rectangle rotated about its center of mass.

steel thickness increases mass-moment of area and directly increases the overall hinge stiffness. Similarly, an increase in offset angle also increases the mass-moment of area and increases stiffness. Using beam bending, the stiffness of the 0° system was calculated to be 0.036 N-m/rad, comparable to our COE and ODE solutions of 0.045 and 0.041 N-m/rad, respectively.

From Equation 5, larger offset angles θ were initially predicted to result in a stiffer hinge. However, it was noticed here that stiffness does not increase by more than a factor of four over all offset angles with the 0.005” thickness. This is because the steel in the offset hinges buckle and flatten before the force required to bend the angled beam is reached, thus reducing the system’s stiffness to near the 0° stiffness, as shown in Figure 7. It was found that inducing a 45° offset angle increased the spring steel stiffness from

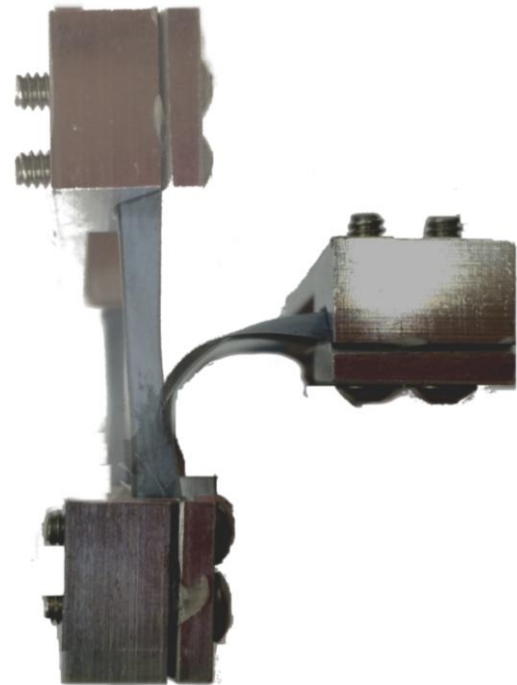


Figure 7. The spring-steel strip flattens as it moves away from the resting position. This in turn reduces the stiffness of the hinge.

0.041 N-m/rad to 0.164 N-m/rad, while increasing the thickness from 0.005 to 0.007 inches increased the stiffness from 0.133 to 0.316N-m/rad. That said, a combination of angle and thickness adjustments are required to change stiffness and tune the hinge to the user’s desired parameters.

5. The Representative Dynamic Model

This section investigates material characteristics found in the solid-state hinge design, specifically the dynamic characteristics of the stiffness and damping over the entire deployment duration, not just the first

oscillation. The solid-state hinge outputs a range of responses based on the offset configuration (see Figure 10 for a comparison). The current analysis begins with determining the kinetic energy in the system, and relating that to the settling time. This section concludes with insight into the non-linear behavior of the solid-state hinge, a deviation from using linear modes as the basis for analysis.

5.1. Deployment Settling

In the solid-state hinge, the dampening component is coupled with the offset angle, angular velocity, and the stiffness of the hinge. Therefore, to gain insight on the dampening effects and dissipation of stored spring energy, the study evaluated how the kinetic energy (KE) changes over time.

As discussed previously, KE can be derived from angular velocity using position data. The maximum KE for each oscillation occurs when velocity approaches a local maximum, i.e. when position crosses the origin. There are two local maximums of KE per period of oscillation, one in each deployment direction. A plot of the maximum KE for the 3U systems and the 1U-0° system is shown in Figure 8. Values decrease exponentially across each half-oscillation, and an exponential curve was fit using a least squares method.

$$KE(t) = KE_o \times \exp\left(-\frac{t}{\tau}\right) \quad (6)$$

The time constant, τ , was extracted and averaged across similar systems, and was used to compare the settling times for the five hinge configurations. From Equation 6, it can be seen that τ represents the time it takes the system to transfer $1/e$, or 66%, of its initial stored spring energy to the spacecraft structure.

The settling time was expected to decrease with an increasing stiffness due to the dampening coefficient coupled to the hinge stiffness. However, an anomaly occurs for the 3U-30°, where the system damps in less than three seconds, or four-to-six oscillations. A similar phenomena is observed on the 1U-15°, where the

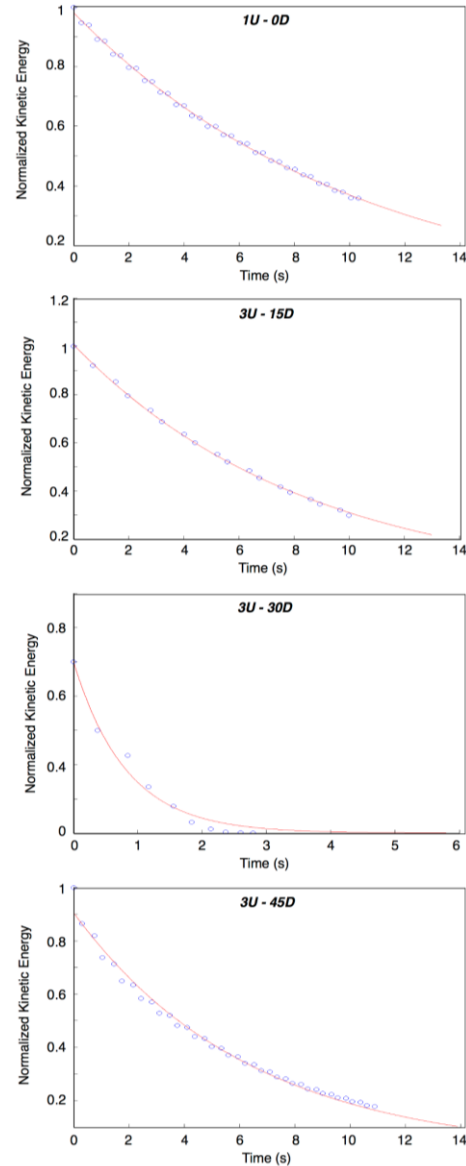


Figure 8. An example of the KE versus time for single deployment under each configuration. An exponential curve is fitted to the data and the time constant τ is extracted.

dampening time is less than other 1U configurations, but is expected to be larger due to less stiffness in the 15° offset. It is concluded that c and k are coupled, and there exists unique angle offsets, thickness, and mass combinations that yield a response similar to a critically damped linear MSD. The remaining hinge systems have a shorter settling time with an increase in system stiffness.

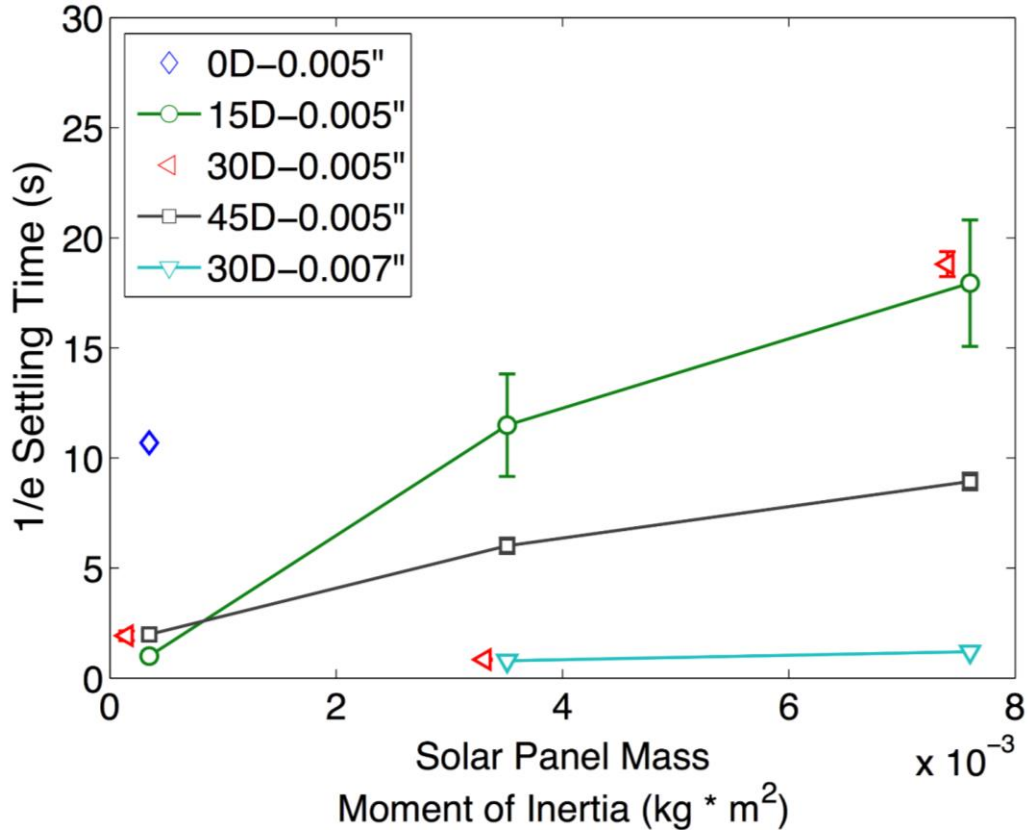


Figure 9. One time constant into the decay of kinetic energy of each hinge configuration. Generally, as solar panel mass increases, time constant increases. The plotted lines demonstrate trending, and error bars represent one standard deviation of the data.

5.2. Nonlinear Characteristics

Again, the Mass-Spring-Dashpot (MSD) system, $m\ddot{x} + c\dot{x} + kx = 0$, was employed to gain insight of non-linear behaviors found in the solid-state hinge. Throughout this paper, peculiarities arose in the offset spring steel configuration, suggesting that the system behaves nonlinearly throughout deployment. Examinations of the linear position vs. time response in Figure 10 of the 1U-0° "linear" configuration and the 3U mass system indicate that deviations exist in the two common MSD properties: a constant oscillation frequency f_n , defined by

$$f_n = \sqrt{\frac{k}{m}}$$

and an exponential decay caused by dampening that takes the form

$$\exp(-2\pi\zeta f_n t)$$

where ζ is the damping ratio.

$$\zeta = \frac{c}{2\sqrt{mk}}$$

A close look at the 3U-30° deployment response in Figure 11 found f_n to change value over the course of deployment and asymmetric dampening.

The varying frequency can be explained by looking at the definition of the natural frequency,

$$f_n = \sqrt{\frac{K}{4\pi^2 m}}$$

and observing how the spring-steel flattens as it moves away from the origin (see Figure 7). The flattening reduces the stiffness, which in turn reduces f_n .

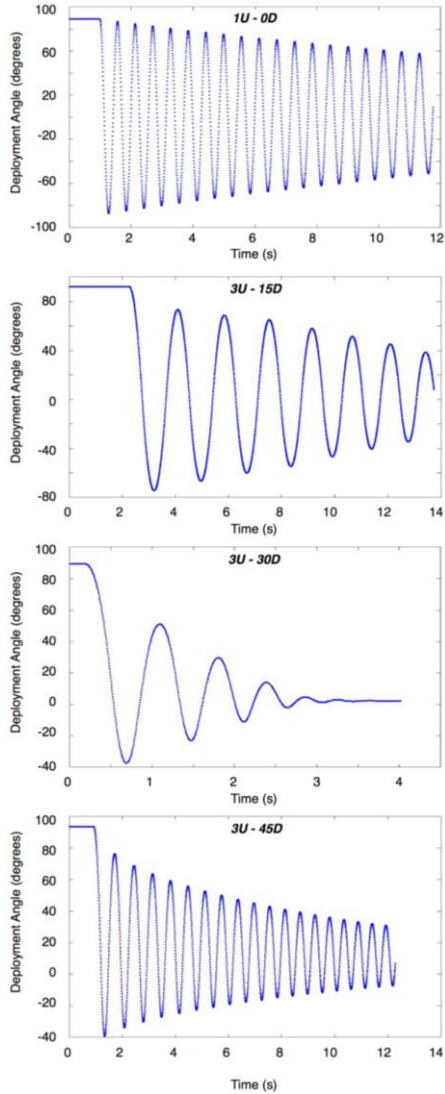


Figure 10. Plotted data comparing four hinge configurations, including the 0° linear system. System response and nonlinearities vary, depending on the offset angle chosen.

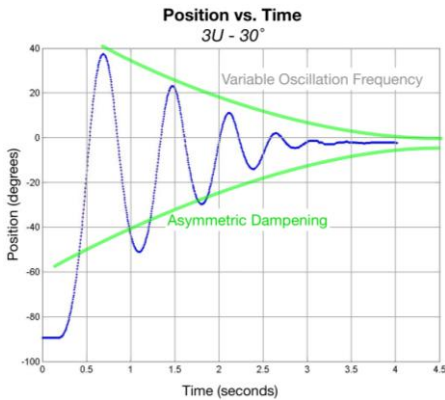


Figure 11. 3U-30° position vs. time. The grid lines and green lines have been added to show the asymmetry of our angled hinges and non-constant spring constant.

Another interesting irregularity due to the correlation between position and stiffness is what happens to the stiffness term near the origin. In Figure 12, the stiffness is calculated over a five point window using the

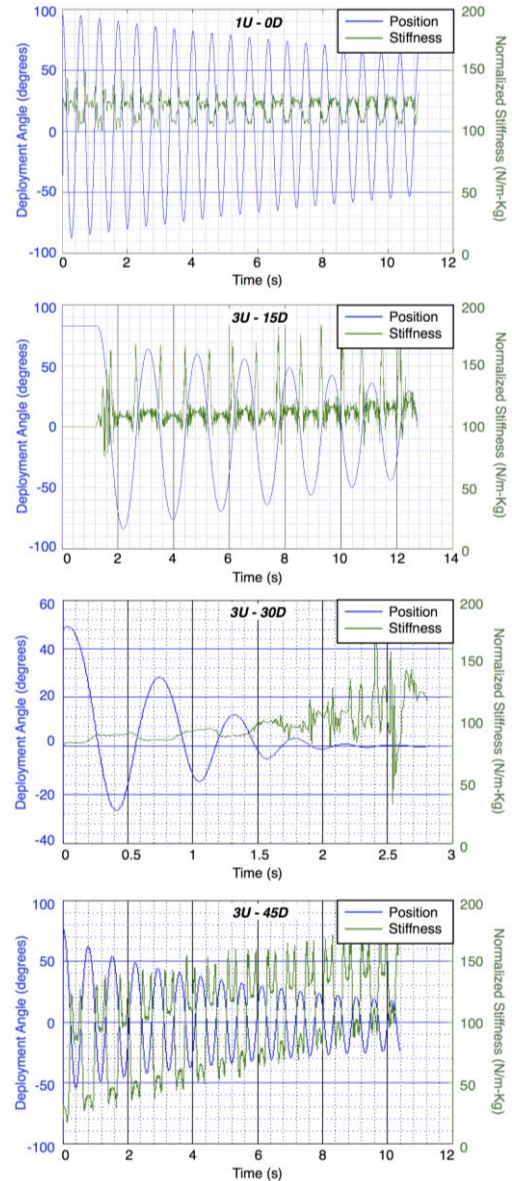


Figure 12. Stiffness vs Position.

same pseudoinverse method described in Section 4, and overlaid with the position data for the corresponding deployment. One can observe a spike in stiffness as the solar panel crosses the origin and the spring-steel unbuckles into a locked state. It appears that this locking stiffness is also evident at the end of the oscillation when the displacements become very small, as

shown in the 3U-30° stiffness plot, but may also be due to the low signal-noise-ratio as the panel approaches zero displacement.

6. ANDESITE Implementation

The nucleation of this idea stemmed from engineering students at Boston University developing a 6U CubeSat, as part of the AFRL-UNP and NASA-ELANA education programs. The 6U satellite ANDESITE (Ad-Hoc Network Demonstration for Extended Satellite-based Inquiry and other Team Endeavors) will investigate the filamentary current structures within the Birkeland regions using a distributed network of orbital magnetometers deployed during a solar storm.

ANDESITE will deploy two 1x3U solar panels to provide adequate power for the science mission. Figure 13 is a 30° demonstration of the solid-state hinge integrated into the structure. The ANDESITE team se-

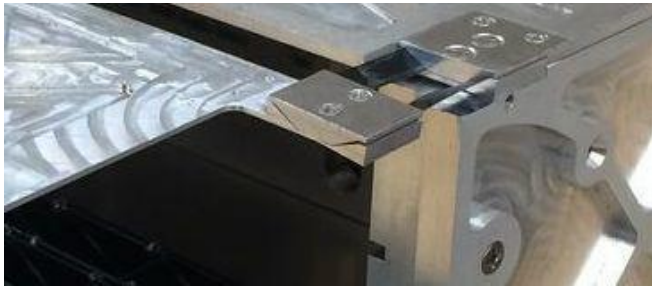


Figure 13. 30° Solid-State hinge configuration integrated into the ANDESITE 6U CubeSat.

lected the 30° configurations for its quick dampening time as found from the microgravity test results.

It should be pointed out that this spring steel hinge implementation does not account for stowing the solar panel to the spacecraft structure during launch. Retraining the solar panel from launch due to G-forces and vibrations is performed by a separate kinematic mount and Frangibolt system, the design details for which are outside the scope of this paper.

In addition to the ANDESITE mission, the Boston University CubeSat program plans to use the solid-state hinge on future projects. By developing an easily

re-purposed design, costs and testing time will be considerably reduced.

7. Conclusions

This paper presents a novel solid-state hinge for solar panel deployment for CubeSats on a university budget, characterizing 12 hinge-mass configurations and presenting their stiffness, settling time, and energy attributes. The analysis herein showed that the solid-state hinge transitions from a near linear system to a fast decaying system, and then finally the transition to an asymmetrical-oscillating non-linear system. It is concluded that the solid-state hinge design can be characterized by one of three phases: 1) underdamped near-linear; 2) near critically damped; and 3) underdamped non-linear. These three phases are due to mechanical coupling of the dampening and stiffness coefficients caused by using two off-planar spring steel strips to provide the actuation, dampening and locking. It is further concluded that increasing the thickness of the off-planar steel strips is the most effective way to increase stiffness and there exists an optimum set of stiffness, dampening, and mass parameters that critically damp the system. Successful deployment of the solid-state hinge on ANDESITE will raise its Technology Readiness Level to 7.

Acknowledgments

Machining and fabrication was conducted at the Boston University (BU) Engineering Product Innovation Center (EPIC) with the help of the EPIC staff. Benchtop testing was performed at the BU College of Arts and Science Center for Space Physics lab. The microgravity campaign was sponsored by the NASA Flight Opportunity Program and the NASA Reduced Gravity Office. This work has been supported by the BU Department of Mechanical Engineering, the BU Department of Electrical Engineering, the BU Center for Space Physics, and the Airforce Research Laboratory Grant as part of the University Nanosatellite Program (Rounds 7 and 8). The following individuals participated in parts of the planning, testing, and analysis: Nathan Darling, Professor Joshua Semeter, Professor

Gregory McDaniel, Professor Paul Barbone, Professor Enrique Gutierrez-Wing, Nate Hepler, and Yamaan Ziade.

References

- Birkeland, K. (1913): *The Norwegian Aurora Polaris Expedition 1902–1903, Volume 1: On the Cause of Magnetic Storms and the Origin of Terrestrial Magnetism*. London, UK: Longmass, Green and Co.
- ClydeSpace. (2014): Clyde Space Solar Panel Masses. Available at: http://www.clyde-space.com/CubeSat_shop/solar_panels (accessed November 20, 2014).
- HoneybeeRobotics. (2006): Solar Array Deployment Systems. Available at: <http://www.honeybeerobotics.com/portfolio/solar-array-deployment-systems/> (accessed November 17, 2014).
- Germain, F., Lathuiliere, M., and Sicre, J. (2009): Deployment of Appendices Using “Maeva” Hinges: Progress in Dynamic Models, in *Proc. 13th European Mechanisms and Tribology Symposium*, Vienna, Austria, ESA Publications Division.
- Givois, D., Sicre, J., and Emerit, A. (2005): Application of “Maeva” Hinge to Myriade Microsatellites Deployment Needs, in *Proc. 11th European Mechanisms and Tribology Symposium*, Lucerne, Switzerland, ESA Publications Division.
- GOMSpace. (2014): Gom Space Solar Panel Masses. Available at: <http://gomspace.com/index.php?p=products-p110> (accessed November 20, 2014).
- Lefort, T. et al. (2002): Low-Cost Hinge for Deployable Structures. Ph.D. thesis, Dept. of Engineering, University of Cambridge, Cambridge, UK.
- Marshek, K. and Juvinall, R. (2012): *Fundamentals of Machine Component Design*, Hoboken, NJ: John Wiley & Sons, Inc.
- Seffen, K. A. and Pellegrino, S. (1997): Deployment of a Rigid Panel by Tape-Springs. Ph.D. thesis, Dept. of Engineering, Univ. of Cambridge, Cambridge, UK.
- Seffen, K. A. and Pellegrino, S. (1999): Deployment Dynamics of Tape Springs, in *Proc., The Royal Society*, London, UK. DOI: 10.1098/rspa.1999.0347.
- Skrobot, G. (2011): Elana – Educational Launch of Nanosatellite: Enhance Education Through Space Flight, in *Proc. of the AIAA/USU Conf. on Small Satellites*, Logan, UT.
- Skrobot, G. and Coelho, R. (2012): Elana – Educational Launch of Nanosatellite: Providing Routine Rideshare Opportunities, in *Proc. of the AIAA/USU Conf. on Small Satellites*, Logan, UT.
- Straub, J. (2012): CubeSats: A Low-cost, Very High-return Space Technology, presented at Reintegrating Space Conf. 2012, Los Angeles, CA, May.